



Title	Spin-density-wave transition of (TMTSF) ₂ PF ₆ at high magnetic fields
Author(s)	Matsunaga, N.; 松永, 悟明; Yamashita, K. et al.
Citation	PHYSICAL REVIEW B, 64(5), 052405 https://doi.org/10.1103/PhysRevB.64.052405
Issue Date	2001-08-01
Doc URL	https://hdl.handle.net/2115/5744
Rights	Copyright © 2001 American Institute of Physics
Type	journal article
File Information	PRB64-5.pdf



Spin-density-wave transition of $(\text{TMTSF})_2\text{PF}_6$ at high magnetic fields

N. Matsunaga, K. Yamashita, H. Kotani, and K. Nomura
Division of Physics, Hokkaido University, Sapporo 060-0810, Japan

T. Sasaki
IMR, Tohoku University, Sendai 980-8577, Japan

T. Hanajiri, J. Yamada, S. Nakatsuji, and H. Anzai
Department of Material Science, Himeji Institute of Technology, Kamigohri 678-1297, Japan
 (Received 28 November 2000; revised manuscript received 22 March 2001; published 13 July 2001)

The transverse magnetoresistance of the Bechgaard salt $(\text{TMTSF})_2\text{PF}_6$ has been measured for various pressures, with the field up to 24 T parallel to the lowest-conductivity direction c^* . A quadratic behavior is observed in the magnetic-field dependence of the spin-density-wave (SDW) transition temperature T_{SDW} . With increasing pressure, T_{SDW} decreases and the coefficient of the quadratic term increases. These results are consistent with the prediction of the mean-field theory based on the nesting of the quasi-one-dimensional Fermi surface. Using a mean-field theory, T_{SDW} for the perfect nesting case is estimated as about 16 K. This means that even at ambient pressure where T_{SDW} is 12 K, the SDW phase of $(\text{TMTSF})_2\text{PF}_6$ is substantially suppressed by the two dimensionality of the system.

DOI: 10.1103/PhysRevB.64.052405

PACS number(s): 75.30.Fv, 72.15.Gd, 74.70.Kn

I. INTRODUCTION

The Bechgaard salts $(\text{TMTSF})_2X$, where TMTSF denotes tetramethyltetraselenafulvalene and $X = \text{PF}_6$, AsF_6 , ClO_4 , etc., have a rich phase diagram exhibiting spin-density-wave (SDW), metallic, superconducting, and field-induced SDW (FISDW) phases depending on pressure or anion kind.¹ The stacking of the TMTSF molecules provides a highly anisotropic Fermi surface only consisting of open sheets. For $(\text{TMTSF})_2\text{PF}_6$, the SDW transition occurs at 12 K at ambient pressure. With increasing pressure, the SDW phase is suppressed and the superconducting phase is induced at 1.1 K above the critical pressure of 0.8 GPa.

The phase diagram of the metallic-SDW and FISDW transitions for the PF_6 salt is well explained by the mean-field theory based on the nesting of the slightly warped, quasi-one-dimensional Fermi surface. When the magnetic field is applied to the SDW state suppressed by the imperfect nesting of the Fermi surface, the total energy of the SDW is lowered by the quantization of the closed orbits near the Fermi level. This corresponds to the fact that the one-dimensional character of electron band is recovered in the magnetic field. It has been predicted that T_{SDW} increases nearly quadratically with the field in low magnetic fields and shows a saturation behavior to the transition temperature for the perfect nesting case in high magnetic fields.² The magnetic-field dependence of T_{SDW} is quite sensitive to the degree of the one-dimensional character of the electron band, i.e., the imperfect nesting of the Fermi surface. Accordingly, the behavior of the SDW phase in the magnetic field gives important information about the stabilization mechanism and the characteristic energy of the SDW state.

In this paper, we present the results of resistivity measurements for the SDW phase of $(\text{TMTSF})_2\text{PF}_6$ under pressure and strong magnetic fields. We discuss an applicability of the mean-field predictions and estimate the characteristic energy of $(\text{TMTSF})_2\text{PF}_6$ from the data using the mean-field theory.

II. EXPERIMENTS

Single crystals of $(\text{TMTSF})_2\text{PF}_6$ were synthesized by the standard electrochemical method. Resistance measurements along the conducting a axis were carried out using a standard four-probe dc method. The typical size of the sample was $1 \times 0.1 \times 0.1 \text{ mm}^3$. Electric leads of 10 μm gold wire were attached with silver paint onto gold evaporated contacts. The current contacts covered the whole areas of both ends of the sample for a uniform current. The temperature was measured using a Cernox CX-1050-SD resistance thermometer calibrated by a capacitance sensor in magnetic fields. The sample was mounted inside a beryllium-copper clamp cell with Daphne 7373 oil as a pressure medium. It is known that the pressure decreases with decreasing temperature and the pressure reduction from 300 K to 4.2 K is approximately 0.15 GPa, irrespective of the initial pressure at 300 K in the present experimental configuration.³ The measurements reported here were carried out on two samples in fields to 24 T (sample 1) in a hybrid magnet at the High Magnetic Field Laboratory, IMR, Tohoku University and in fields to 16 T (sample 2) in a superconducting magnet at Hokkaido University.

III. RESULTS AND DISCUSSION

The temperature dependence of the transverse resistance in $(\text{TMTSF})_2\text{PF}_6$ for various pressures is shown in Fig. 1. For every pressure, the resistance shows a steep increase associated with the metal-SDW transition. The SDW transition temperature T_{SDW} is determined from the peak position in the derivative of the logarithm of these data with $1/T$. The peak height at T_{SDW} decreases with increasing pressure. Although the transition width, which is estimated from the peak width in the derivative curve, is broadened with decreasing T_{SDW} , the peak is fairly sharp at every pressure. The temperature and pressure dependencies of the resistance are con-

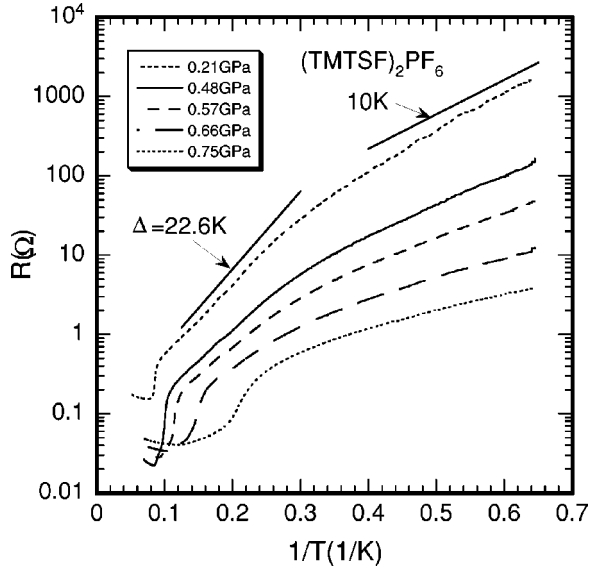


FIG. 1. Temperature dependence of the transverse resistance in $(\text{TMTSF})_2\text{PF}_6$ for various pressures. Data are for sample 2. The straight lines show the apparent activation behavior.

sistent with previous results.⁴ More detailed behaviors of the resistance will be discussed later.

Figure 2 shows the temperature dependence of the transverse magnetoresistance with the field B parallel to the lowest-conductivity direction c^* at 0.48 GPa. In each field, the resistance shows a steep increase, associated with the SDW transition, with decreasing temperature. From this figure, it is clear that the transition is shifted towards higher temperatures as the field is increased. We determine T_{SDW} from the peak in the derivative of the logarithm of the resistance with $1/T$, which is also shown in Fig. 2. The field dependence of T_{SDW} is shown in Fig. 3. At 0.48 GPa, T_{SDW} increases from 9.8 K in zero field up to 11.4 K at 24 T. This field dependence of T_{SDW} is well described by the quadratic behavior as

$$T_{\text{SDW}}(B) = T_{\text{SDW}}(0) + CB^2, \quad (1)$$

with a constant C . The solid line in Fig. 3 is the best fit of the quadratic function to the experimental data. The observed result for T_{SDW} is well described by a quadratic behavior and there is no saturation even at 24 T.

Figure 4 shows the magnetic-field dependence of T_{SDW} for various pressures. With increasing pressure, T_{SDW} decreases and the coefficient C of the quadratic term increases. These results are qualitatively consistent with the prediction of the mean-field theory.² The solid line in Fig. 4 is also the best fit of the quadratic function to experimental data. We obtain the coefficient C from the fitting and summarize the relation between T_{SDW} and the coefficient C in log-log scale in Fig. 5. We also plot the earlier data for $(\text{TMTSF})_2\text{PF}_6$ for comparison.⁵⁻⁷ There is good agreement between the present result and previous ones, although a slight scatter is seen in the high pressure.

From the observed curvature of the coefficient C of the quadratic term as a function of T_{SDW} for various pressures,

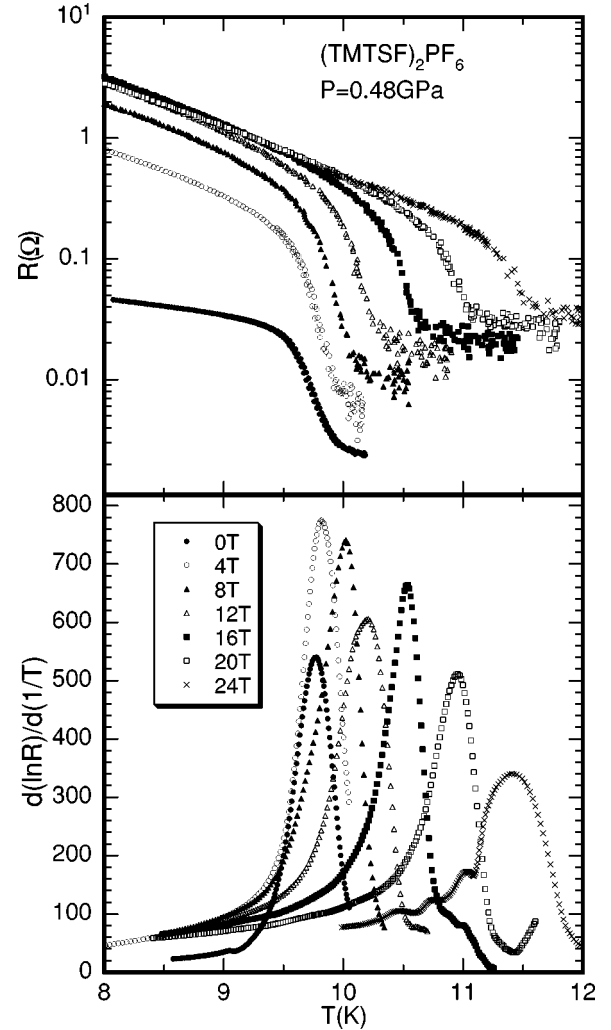


FIG. 2. (Top) Temperature dependence of the transverse magnetoresistance in $(\text{TMTSF})_2\text{PF}_6$ at 0.48 GPa in a constant field along the c^* axis as indicated. (Bottom) Logarithmic derivatives of the data. Data are for sample 1.

we can determine several important parameters for the SDW transition in a mean-field theory.⁸⁻¹⁰ The dashed line in Fig. 5 is the fit of this theory to the experimental data under low pressure and the agreement is good. The fit gives T_{SDW} corresponding to the perfect nesting case as $T_{\text{SDW}0} = 16$ K and Fermi velocity $v_F = 1.03 \times 10^5$ m/s, with a lattice parameter along the b' axis of 7.7×10^{-10} m. From these parameters, we can determine the imperfect nesting parameter ϵ_0/Δ_0 where ϵ_0 is the energy parameter characterized by the deviation from perfect nesting and Δ_0 is the SDW order parameter at $T=0$ K for $\epsilon_0=0$. At ambient pressure where T_{SDW} is 12 K, we obtain $\epsilon_0/\Delta_0 = 0.8$ for $(\text{TMTSF})_2\text{PF}_6$. Although the value of ϵ_0/Δ_0 is somewhat large in comparison with previous estimates,⁴ this parameter is consistent with the value estimated from the analysis of the scanning tunnel microscope (STM) spectroscopy.¹¹ We summarize the value of T_{SDW} and ϵ_0/Δ_0 obtained from this fit for various pressures in Table I. It should be noted that even at ambient pressure where T_{SDW} is 12 K, the SDW phase of $(\text{TMTSF})_2\text{PF}_6$ is

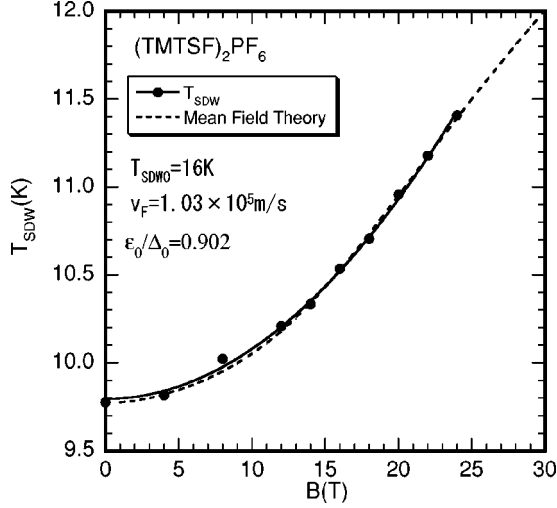


FIG. 3. Magnetic-field dependence of the SDW transition temperature T_{SDW} at 0.48 GPa. The full line is the best fit of the quadratic function. The dashed line is the fit using mean-field theory.

substantially suppressed by the two dimensionality of the system.

According to a more general description for the SDW in the magnetic field based on the mean-field theory,^{8,9} the magnetic-field dependence of T_{SDW} is described by

$$\ln \left[\frac{T_{SDW}(B)}{T_{SDW_0}} \right] \approx \sum_{l=-\infty}^{\infty} J_l^2 \left(\frac{\epsilon_0}{\omega_b} \right) \times \left\{ \text{Re} \Psi \left(\frac{1}{2} + \frac{il\omega_b}{2\pi T_{SDW}} \right) - \Psi \left(\frac{1}{2} \right) \right\}, \quad (2)$$

where J_l and Ψ are Bessel and digamma functions, respectively, $\omega_b = v_F e b' B$ is the cyclotron frequency along the b' axis, and e is the electron charge. The dashed line in Fig. 3 is the curve calculated from Eq. (2) using the above parameters. The experimental results are well reproduced by the

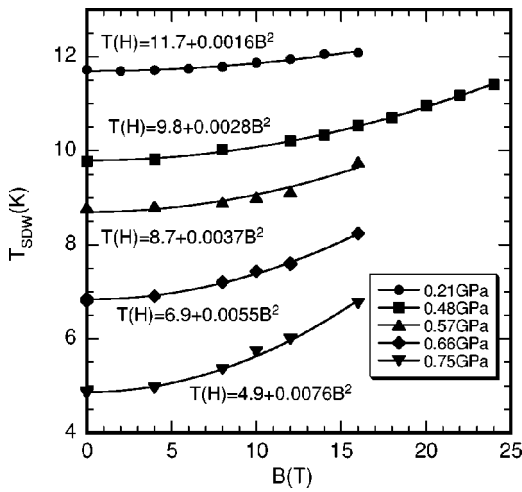


FIG. 4. Magnetic-field dependence of the SDW transition temperature T_{SDW} for various pressures. The full line is the best fit of the quadratic function.

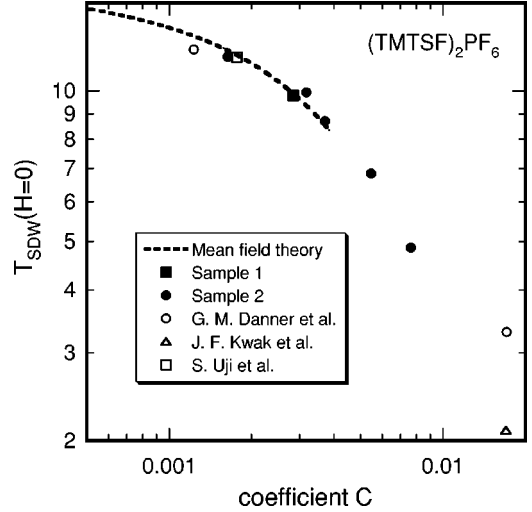


FIG. 5. T_{SDW} vs coefficient C of a quadratic term for $(TMTSF)_2PF_6$, together with C for previous results (Refs. 5 and 6). The dashed line is the fit of mean-field theory.

mean-field calculation, indicating that the values obtained for these parameters are reasonable. The mean-field calculations nicely account for the field-induced increase of T_{SDW} and explain the absence of saturation behavior in the present experimental range of magnetic field as shown in Fig. 3. Although the value of Fermi velocity is somewhat small in comparison with a previous estimate $v_F = 1.5 \times 10^5$ m/s from the resistance measurements, which assumed that $(TMTSF)_2PF_6$ at ambient pressure was the perfect nesting case,⁴ these parameters are consistent with the fact that there is no deviation from the quadratic behavior of T_{SDW} up to 28 T at ambient pressure.^{5,7}

Finally, we discuss the temperature and pressure dependencies of the resistance. As shown in Fig. 1, the transverse resistance roughly shows an activation-type temperature dependence below T_{SDW} , however, the situation is much more complex than in the usual activated insulator. The slope of the resistance against $1/T$ that corresponds to the apparent activation energy slowly decreases from $\Delta = 22.6$ K at $0.5T_{SDW}$ to $\Delta = 10.0$ K below 2 K under 0.21 GPa. These results are consistent with previous results.⁷ Usually, one would expect that the activation energy is simply given by the minimum value of the gap, as $\Delta_M = \Delta_0 - \epsilon_0$. With $T_{SDW_0} = 16$ K, $\epsilon_0/\Delta_0 = 0.794$, and the mean-field BCS relation for the weak-coupling limit as $2\Delta_0 = 3.5k_B T_{SDW_0}$, we obtain the direct gap $2\Delta_0 = 56$ K and $\Delta_M = 5.6$ K for 0.21

TABLE I. SDW transition temperature T_{SDW} and imperfect nesting parameter ϵ_0/Δ_0 at five different pressures.

P (GPa)	T_{SDW} (K)	ϵ_0/Δ_0
0.21	11.7	0.794
0.48	10.0	0.889
0.57	8.8	0.935
0.66	6.9	0.979
0.75	4.9	0.997

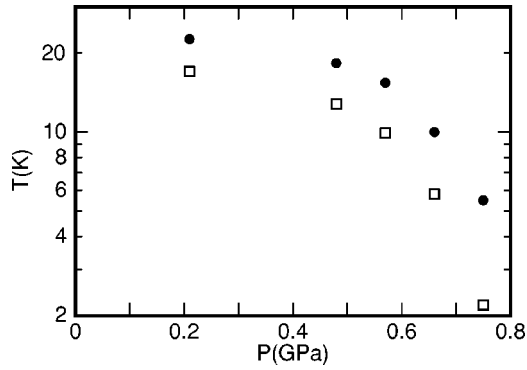


FIG. 6. Pressure dependence of the apparent activation energy at $0.5T_{SDW}$ (●) and the geometrically averaged activation energy Δ_G (□) (see text).

GPa. Although the value of $2\Delta_0$ is somewhat small in comparison with a previous estimate from an optical measurement, where $2\Delta_0 = 101$ K,^{12,13} this value is consistent with the value estimated from the analysis of the STM spectroscopy, where $2\Delta_0 = 58 \sim 67$ K.¹¹ The value of Δ_M is much smaller than the obtained value from the resistance at $0.5T_{SDW}$. The activation-type temperature dependence with the minimum value of the gap is correct only well below the temperature corresponding to the activation energy Δ_M . Above and around this temperature, the temperature dependence of the resistance is better defined by considering the geometrically averaged activation energy of the state density⁹ as

$$\Delta_G = \sqrt{\Delta_0^2 - \epsilon_0^2}. \quad (3)$$

From this definition, we obtain the geometrically averaged activation energy $\Delta_G = 17$ K for 0.21 GPa. This value is close to the value of the apparent activation energy around $0.5T_{SDW}$. The slow decrease of the apparent activation energy with decreasing temperature can be explained by the crossover from the geometrically averaged activation energy Δ_G to the activation energy Δ_M . With increasing pressure, the apparent activation energy Δ at $0.5T_{SDW}$ decreases from 22.6 K for 0.21 GPa to 5.5 K for 0.75 GPa. These results are also consistent with previous results.⁴ With increasing pressure, the ratio of the apparent activation energy at $0.5T_{SDW}$ to Δ_G becomes large as shown in Fig. 6. According to the mean-field theory, the temperature dependence of or-

der parameter becomes stronger with increasing two dimensionality of the electron band and an increase in order parameter with decreasing temperature gives a steep decrease in the number of electrons activated across the gap.¹⁰ As a result, the apparent activation energy modified by the temperature dependence of the order parameter increases with increasing pressure and the pressure dependence of the ratio of the apparent activation energy at $0.5T_{SDW}$ to Δ_G can be explained by this temperature dependence of the order parameter. Finally, the temperature dependence of the resistance below T_{SDW} is successfully explained by the mean-field theory with the same parameters as in the discussion for T_{SDW} .

IV. CONCLUSION

We have measured the resistivity in the SDW phase of $(TMTSF)_2PF_6$ under various pressures and magnetic fields parallel to the c^* axis. The SDW transition temperature in zero field decreases with increasing pressure. When the magnetic field is applied to this SDW phase suppressed by the pressure, T_{SDW} recovers its value. The field dependence of T_{SDW} is described by a quadratic behavior and the coefficient of the quadratic term increases with increasing pressure. These results are consistent with the prediction of the mean-field theory based on nesting of the Fermi surface. We have determined the SDW transition temperature for the perfect nesting case as $T_{SDW_0} = 16$ K and the imperfect nesting parameter $\epsilon_0/\Delta_0 = 0.8$ for $(TMTSF)_2PF_6$ at ambient pressure. This means that the SDW phase of $(TMTSF)_2PF_6$ at ambient pressure, whose T_{SDW} is 12 K, is suppressed by the two dimensionality of the system. The temperature and pressure dependencies of the activation energy in the SDW phase of $(TMTSF)_2PF_6$ are also well explained by the mean-field theory using the same characteristic energy in the SDW state by taking into account the geometric average of the state density.

ACKNOWLEDGMENTS

We would like to thank Professor K. Murata for technical advice on the high-pressure measurement. Some of this work was carried out as part of the ‘‘Research for the Future’’ project, JSPS-RFTF97P00105, supported by the Japan Society for the Promotion of Science.

¹For a review, see T. Ishiguro, K. Yamaji, and G. Saito, *Organic Superconductors II* (Springer-Verlag, Berlin, 1998).

²G. Montambaux, Phys. Rev. B **38**, 4788 (1988).

³K. Murata *et al.*, Rev. Sci. Instrum. **68**, 2490 (1997).

⁴N. Biškup, S. Tomić, and D. Jérôme, Phys. Rev. B **51**, 17 972 (1995).

⁵G.M. Danner, P.M. Chaikin, and S.T. Hannahs, Phys. Rev. B **53**, 2727 (1996).

⁶J.F. Kwak *et al.*, Phys. Rev. Lett. **56**, 972 (1986).

⁷S. Uji *et al.*, Phys. Rev. B **55**, 12 446 (1997).

⁸A. Bjeliš and K. Maki, Phys. Rev. B **45**, 12 887 (1992).

⁹K. Maki, Phys. Rev. B **47**, 11 506 (1993).

¹⁰K. Yamaji, J. Phys. Soc. Jpn. **51**, 2787 (1982).

¹¹K. Ichimura *et al.*, Synth. Met. **103**, 2097 (1999).

¹²G. Mihály, A. Virosztek, and G. Grüner, Phys. Rev. B **55**, R13 456 (1997).

¹³V. Vescoli *et al.*, Phys. Rev. B **60**, 8019 (1999).